Neuron, Vol. 42, 237–251, April 22, 2004, Copyright ©2004 by Cell Press

The Synaptic Vesicle Protein CSPα Prevents Presynaptic Degeneration

Rafael Fernández-Chacón,[1,2] Markus Wölfel,[5] Hiroshi Nishimune,[7] Lucia Tabares,[2] Frank Schmitz,[3,4] Manuel Castellano-Muñoz,[2] Christian Rosenmund,[6] Maria L. Montesinos,[2] Joshua R. Sanes,[7] Ralf Schneggenburger,[5] and Thomas C. Südhof[1,*]

[1]Center for Basic Neuroscience
Department of Molecular Genetics and
Howard Hughes Medical Institute
University of Texas Southwestern Medical Center
Dallas, Texas 75390
[2]Departamento Fisiología Médica y Biofísica
Universidad de Sevilla
Avenida Sánchez-Pizjuán 4
41009-Sevilla
Spain
[3]Universität Leipzig
Institut für Anatomie
Liebigstrasse 13
04103 Leipzig
Germany
[4]Institut für Anatomie und Zellbiologie
Universität des Saarlandes Homburg/Saar
Germany
[5]AG Synaptic Dynamics and Modulation
[6]AG Synaptic Physiology
Department of Membrane Biophysics
MPI für biophysikalische Chemie
37070 Göttingen
Germany
[7]Department of Anatomy and Neurobiology
Washington University School of Medicine
660 South Euclid Avenue
St Louis, Missouri 63110

Summary

Cysteine string protein α (CSPα)—an abundant synaptic vesicle protein that contains a DNA-J domain characteristic of Hsp40 chaperones—is thought to regulate Ca^{2+} channels and/or synaptic vesicle exocytosis. We now show that, in young mice, deletion of CSPα does not impair survival and causes no significant changes in presynaptic Ca^{2+} currents or synaptic vesicle exocytosis as measured in the Calyx of Held synapse. At 2–4 weeks of age, however, CSPα-deficient mice develop a progressive, fatal sensorimotor disorder. The neuromuscular junctions and Calyx synapses of CSPα-deficient mice exhibit increasing neurodegenerative changes, synaptic transmission becomes severely impaired, and the mutant mice die at ~2 months of age. Our data suggest that CSPα is not essential for the normal operation of Ca^{2+} channels or exocytosis but acts as a presynaptic chaperone that maintains continued synaptic function, raising the possibility that enhanced CSPα function could attenuate neurodegenerative diseases.

*Correspondence: thomas.sudhof@utsouthwestern.edu

Introduction

When an action potential invades a presynaptic nerve terminal, voltage-gated Ca^{2+} channels open, and Ca^{2+} entering the terminal triggers neurotransmitter release by synaptic vesicle exocytosis (Katz, 1969). Empty synaptic vesicles then undergo endocytosis to recycle for a new round of exocytosis. Synaptic vesicle exo- and endocytosis are mediated by a sophisticated apparatus that turns nerve terminals into membrane trafficking machines. Presynaptic terminals widely differ in ultrastructural appearance, neurotransmitter type, and use-dependent plasticity, but all terminals share the same functional architecture that depends on the autonomous, Ca^{2+}-regulated exo- and endocytosis of synaptic vesicles. Since synaptic vesicles are the central organelles in neurotransmitter release, the characterization of synaptic vesicle proteins is an important goal in understanding synaptic function. This goal has been largely achieved for cataloging synaptic vesicle proteins but is far from complete for the functional understanding of these proteins (reviewed in Fernández-Chacón and Südhof, 1999). Among the functions performed by synaptic vesicle proteins, exo- and endocytosis are relatively easy to measure, while other stages of the vesicle cycle—e.g., the biogenesis and recycling or synaptic vesicles or the maintenance of vesicles as separate organelles—are difficult to evaluate. As a result, vesicle proteins that participate in exo- and endocytosis are better understood than proteins involved in other functions. In fact, some of the proteins that are currently thought to participate in exo- or endocytosis may act at a different stage of the vesicle cycle and influence exo- or endocytosis only indirectly.

Cysteine string protein (CSP) is an abundant, evolutionarily conserved synaptic vesicle protein that contains a string of C-terminal cysteine residues (Zinsmaier et al., 1990; Gundersen and Umbach, 1992). In *Drosophila* mutants that lack CSP, most flies die during development, but a small percentage survives into adulthood with a temperature-sensitive paralytic phenotype (Umbach et al., 1994; Zinsmaier et al., 1994). Studies of the neuromuscular junction of larvae from surviving mutant flies revealed that deletion of CSP severely depressed evoked neurotransmitter release at the permissive temperature and nearly abolished release at the nonpermissive temperature (Umbach et al., 1994; Zinsmaier et al., 1994). Based on these results and on studies of vertebrate CSP, three different hypotheses for the function of CSP were proposed.

One hypothesis is that CSP is involved in Ca^{2+} channel function. Gundersen and Umbach (1992) observed that CSP antisense RNA inhibited the expression of N-type Ca^{2+} channels when coinjected with Torpedo electric lobe mRNA into *Xenopus* oocytes. The connection of CSP to Ca^{2+} channels was strengthened by the finding

that voltage-gated Ca^{2+} influx was impaired in CSP mutant *Drosophila* synapses and that neurotransmitter release could be rescued in these flies by application of a Ca^{2+} ionophore (Ranjan et al., 1998; Umbach et al., 1998). Furthermore, introduction of recombinant CSP into chick nerve terminals increased Ca^{2+} channel activity (Chen et al., 2002), and CSPα may bind to vertebrate Ca^{2+} channel proteins (Leveque et al., 1998) or to G protein subunits regulating Ca^{2+} channels (Magga et al., 2000). The idea that CSP mediates the assembly or regulation of Ca^{2+} channels at the active zone is attractive in view of the localization of CSP on synaptic vesicles. However, this hypothesis was challenged by fluorometric Ca^{2+} measurements that demonstrated that nerve terminals from *Drosophila* CSP mutants display an increase, and not a decrease, in Ca^{2+} influx (Dawson-Scully et al., 2000) and by measurements of Ca^{2+} currents in peptidergic terminals from CSP mutant flies (Morales et al., 1999).

A second hypothesis for CSP function is that CSP directly regulates exocytosis. Consistent with such a role, CSP interacts with syntaxin and synaptotagmin in pulldown experiments (Nie et al., 1999; Evans and Morgan, 2002; however, see Leveque et al., 1998, and Matos et al., 2000, for alternative results). Moreover, transmitter release is depressed in *Drosophila* CSP mutants despite higher than normal Ca^{2+} levels, indicating a role for CSP in determining the Ca^{2+} sensitivity of the secretory apparatus (Dawson-Scully et al., 2000). Furthermore, overexpression of CSP in neuroendocrine cells altered exocytosis but had no effect on Ca^{2+} channel activity (Brown et al., 1998; Graham and Burgoyne, 2000; Chamberlain and Burgoyne, 1998; Zhang et al., 1998).

A third hypothesis for CSP function is based on the observation that CSP contains a DNA-J domain. DNA-J domains are characteristic of cochaperones of the Hsp40 family, and they functionally collaborate with the DNA-K domains of Hsc70 proteins (reviewed in Kelley, 1998; Hartl and Hayer-Hartl, 2002). Indeed, CSP activates the ATPase activity of Hsc70 (Braun et al., 1996; Chamberlain and Burgoyne, 1997) and forms a trimeric complex with Hsc70 and a tetratricopeptide repeat protein called SGT (Tobaben et al., 2001). This complex catalyzes the ATP-dependent refolding of denatured luciferase (Tobaben et al., 2001). A role for CSP as a chaperone to renature nerve terminal proteins that misfold during the continuous operation of the synaptic vesicle cycle is also attractive but is not currently supported by in vivo evidence.

We have attempted to test these hypotheses about the function of CSP by analyzing knockout (KO) mice lacking CSP. We show that mice contain three CSP genes (CSPα, β, and γ), but only CSPα is expressed in brain, whereas CSPβ and CSPγ are testis specific. We demonstrate that CSPα KO mice are relatively normal at birth but exhibit a progressive lethal phenotype that manifests as muscle weakness and a sensorimotor disorder at 2–4 weeks of age. Analysis of synaptic transmission in CSPα KO mice at the Calyx of Held synapse, a preparation that allows electrophysiological measurements of unparalleled resolution, documented that CSPα was not required for Ca^{2+} channel function or Ca^{2+}-triggered exocytosis. Instead, we show that CSPα is essential for the long-term survival of synapses and functions to prevent the degeneration of nerve terminals. These data are consistent with a role for CSPα as a molecular chaperone that makes it possible for synapses to keep running for extended time periods.

Results

KO of CSPα Causes Postnatal Lethality

Sequence analyses revealed that the mouse genome contains three CSP genes encoding CSPα, β, and γ (Supplemental Figure S1 at http://www.neuron.org/cgi/content/full/42/2/237/DC1). Traditionally, only CSPα (which is widely expressed throughout development in most tissues Chamberlain and Burgoyne, 1996) was studied. To determine the expression patterns of CSPβ or γ that could potentially be functionally redundant with CSPα, we used RNA blotting and quantitative RT-PCR. We found that CSPβ and γ mRNAs are abundant in testis but are not detectable in other adult tissues (Supplemental Figure S2) or in brain at all developmental stages tested (P5, P15, and P40; Supplemental Table S1). Thus, in mice, brain contains only CSPα at significant levels, and CSPβ and CSPγ likely do not have a neuronal function.

To generate CSPα KO mice, we isolated genomic clones that contained the first coding exon of the mouse CSPα gene and constructed a targeting vector for homologous recombination (Figure 1A). We electroporated the targeting vector into embryonic stem cells, selected homologous recombinants, and used them to generate CSPα KO mice. Genotyping of newborn offspring from heterozygous matings identified apparently normal heterozygous and homozygous mutant mice that were born in the expected Mendelian ratios (data not shown). Thus, the homozygous CSPα mutation is not pre- or perinatally lethal. As shown by immunoblotting of brain proteins, heterozygous mutant mice contained less CSPα than wild-type controls, while homozygous mutant mice lacked CSPα (Figure 1B). Control proteins such as SCAMP1, complexins, and synaptobrevin 2 exhibited no major change. Quantitative RT-PCR demonstrated that the expression of CSPβ or γ did not increase in brains from CSPα KO mice at P5 or P15, ruling out a compensatory upregulation of other CSP isoforms in the KOs (Supplemental Data and Supplemental Table S1 at http://www.neuron.org/cgi/content/full/42/2/237/DC1). In all of the experiments described here, analyses were carried out with littermates derived from heterozygous matings to exclude confounding background effects.

In the first 2 postnatal weeks, the weight and survival of CSPα KO mice were not significantly different from heterozygous and wild-type littermate controls (Figure 1C). However, at 2–3 weeks of age, the KO mice began to suffer from progressive weakness. After P15, the KO mice stopped gaining weight (Figure 1C). At $\sim$P30, CSPα KO mice entered into a lethargic state but were able to eat and move when stimulated. CSPα KO mice started to die in the third postnatal week, most KO mice perished in the second postnatal month, and none survived beyond 3 months (Figure 1D). Internal examination of KO mice revealed bilateral intraabdominal cryptorchidism

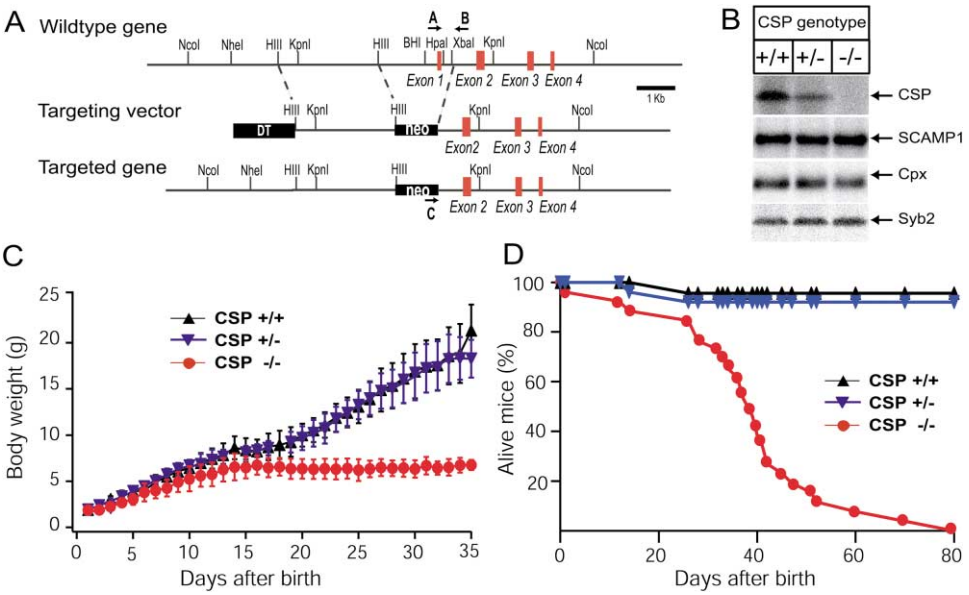

Figure 1. Generation and Characterization of CSPα KO Mice

(A) Schematic diagram of the wild-type CSPα gene, the targeting vector used for homologous recombination, and the KO allele after gene targeting. In the targeting vector, exon 1 encoding residues 1–36 of CSPα was replaced by a neomycin resistance gene (neo) for positive selection. The short arm of the vector was flanked by a diphtheria toxin gene (DT) for negative selection. The positions of strategic restriction sites and of PCR primers ("A," "B," and "C") are indicated. Note that mice contain two additional CSP genes (CSPβ and CSPγ; Supplemental Figure S1 at http://www.neuron.org/cgi/content/full/42/2/237/DC1) that were detectable only in testis and not in brain (Supplemental Figure S2).

(B) Immunoblot analysis of brain proteins from wild-type (+/+), heterozygous (+/−), and homozygous CSPα KO mice (−/−) with antibodies to CSPα, SCAMP1, complexins (Cpx), and synaptobrevin/VAMP 2 (Syb2).

(C) Body weights of wild-type, heterozygous, and homozygous CSPα KO mice as a function of age (n = 23 $CSP^{+/+}$, 25 $CSP^{+/-}$, and 19 $CSP^{-/-}$ mice; data shown are mean ± SD).

(D) Postnatal survival of CSPα KO mice. The survival of the offspring from heterozygous matings is plotted as percent of viable mice remaining as a function of age (n = 23 $CSP^{+/+}$, 25 $CSP^{+/-}$, and 26 $CSP^{-/-}$ mice).

but no other developmental abnormalities (data not shown). Heterozygous mutant and wild-type mice exhibited no differences in body weight or mortality, suggesting that the decrease in CSPα levels in heterozygotes is not sufficient to impair survival.

Impaired Sensorimotor Performance and Neuromuscular Function in CSPα KO Mice

CSPα KO and littermate control mice were subjected to a standard neurological examination (modified SHIRPA protocol; Rogers et al., 1997). In the open field test, CSPα KO mice exhibited a dramatic loss of spontaneous activity that was already apparent at P15 (Figure 2A). The impairment was also present to a lesser degree in heterozygous CSPα mutant mice that were normal in all other parameters examined (Figure 2). CSPα KO mice manifested muscle weakness as evident from a tendency to clasp the hindlimbs when suspended by the tail (data not shown) and a lack of gripping strength on fore- and hindlimbs that was observed as early as P15 (Figure 2B). The KO mice presented a progressively poorer posture, often with the typical leg position of "inverted champagne bottles" and a thin pelvis due to decreased girdle muscle mass. No tremor was evident. CSPα KO mice were unable to stay on a turning rod 30 cm above the floor (Figure 2C) and displayed a poor acoustic startle reflex (data not shown). In addition, already at P15, the CSPα KO mice had difficulties in getting up after they were placed on their right or left backside, with a severe deterioration in this condition after P25 (Figure 2D).

The poor performance of CSPα KO mice in locomotor tests suggested that synaptic transmission at the neuromuscular junction (NMJ) may have been impaired. To examine this, we studied the electromyographic responses in wild-type and CSPα KO mice at P15, P23, and P45 (Figure 2E). In wild-type mice, the mean amplitudes of compound muscle action potentials (CMAPs) were small at P13–P15 but increased ~2-fold at P23 and P45–P47 (Figure 2F and Supplemental Table S2 at http://www.neuron.org/cgi/content/full/42/2/237/DC1). In CSPα KO mice, the mean CMAP amplitudes were similar to wild-type littermate controls at P13–P15 and P23 but dropped significantly at P43–P47. This result indicates an initially robust function at the NMJ which later deteriorates. The defects in neuromuscular synaptic transmission in the CSPα KO mice became even more apparent when we examined responses to short stimulus trains (Figure 2G). In wild-type mice, repetitive stimulation elicited the same amount of maximal depression at P15, P23, and P45 (to 64%–69% ± 5% of initial amplitude). In contrast, we observed enhanced synaptic depression in CSPα KO mice already at P15 (52% ± 5%; n = 4) and even more severe depression at P23 and P45 (to 35% ± 3%, n = 4, and 39% ± 6%, n = 3, respectively; Figure 2G). Together, these data suggest that CSPα KO mice exhibit a limited functional impair-

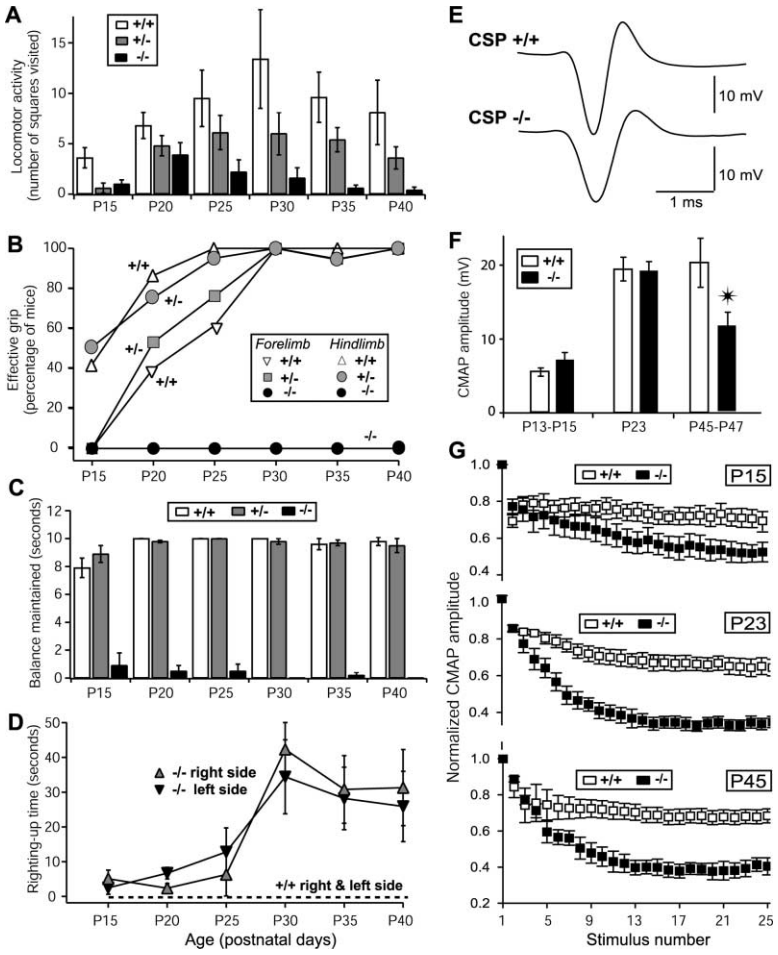

Figure 2. Sensorimotor Deficits in CSPα KO Mice

(A) Spontaneous open field activity of *CSP*$^{+/+}$, heterozygous *CSP*$^{+/-}$, and *CSP*$^{-/-}$ mice. The number of squares touched by all four paws in a 30 s time period was measured at postnatal days P15–P40.

(B) Grip strength of fore- and hindlimbs (see Experimental Procedures). The percentage of mice capable of effectively gripping onto a grid is displayed as a function of postnatal age.

(C) Balance test. Data shown are the times (in seconds) that a mouse can stay on a slowly rotating square thin stick (10 s = maximum).

(D) Righting times. Mice are placed on the right or left back side, and the time required to become upright is measured. Note that wild-type controls achieve an upright position instantaneously (dotted line).

(E) Representative recordings of compound muscle action potentials (CMAPs) from CSPα wild-type and KO mice (P23).

(F) Absolute CMAP amplitudes in response to supramaximal stimulation at P13–15, P23, and P43–P7.

(G) Normalized CMAP amplitudes during supramaximal stimulation (50 Hz for 1 s) at P15, P23, and P45. All data are means ± SEMs.

ment of the NMJ at P15 that becomes severe at P23 and P45.

Degeneration of the NMJ

The weakness of CSPα KO mice indicates that their NMJs might be defective. We used light and electron microscopy to test this possibility. First, to assess the size and shape of the NMJ, we double-stained sections with rhodamine-α-bungarotoxin (to label acetylcholine receptors in the postsynaptic membrane) and antibodies to neurofilaments and SV2 (to label motor axons and nerve terminals). In controls, NMJs were elaborately branched by 3 weeks of age, and each receptor-rich branch of the postsynaptic apparatus was directly apposed by a presynaptic nerve terminal. In mutants, in contrast, the postsynaptic apparatus was less mature, often having a perforated appearance, which corresponds to a transitional form in the development of the "pretzel-shaped" aggregate (Sanes and Lichtman, 1999). Moreover, portions of the postsynaptic apparatus were unoccupied by presynaptic nerve branches, and some nerve branches appeared thinner than normal (Figures 3A and 3B). Because the pre- and postsynaptic apparati develop in parallel, these results imply that the nerve terminal arbor formed normally but then began to degenerate.

Next, we prepared sternocleidomastoid muscles from 3-week-old mice for electron microscopy. In many respects, synaptic ultrastructure was normal in mutants: vesicle-laden nerve terminals abutted an enfolded, electron-dense postsynaptic membrane; synaptic vesicles were clustered at active zones on the presynaptic membrane; and terminals were capped by processes of Schwann cells. Moreover, the numbers of presynaptic active zones and postsynaptic folds did not differ significantly between mutants and controls (Table 1). On the other hand, mutant terminals were strikingly abnormal in two ways. First, 42% (19/45) of terminals contained vacuoles and/or multilamellar bodies, both of which are symptomatic of degenerative processes or defective membrane trafficking (Figures 3F and 3G). Such inclusions were seen in only 6% (2/35) of controls. Second, slender Schwann cell processes invaginated the surface of the nerve terminal at 45% of the sites examined (Figures 3D and 3E). This number is a minimal estimate because we examined only a single section (~0.1 μm thick) from each neuromuscular junction (~30–50 μm diameter), so it is possible that all terminals were invaginated at least once. In contrast, similar but smaller invaginations were seen in only 2/35 control terminals. The aberrant Schwann cell processes found in the CSPα KO mice are quite distinct from those observed in mutants lacking laminin β2 (Patton et al., 1998) or following muscle damage (e.g., Jirmanova, 1975). In those cases, the

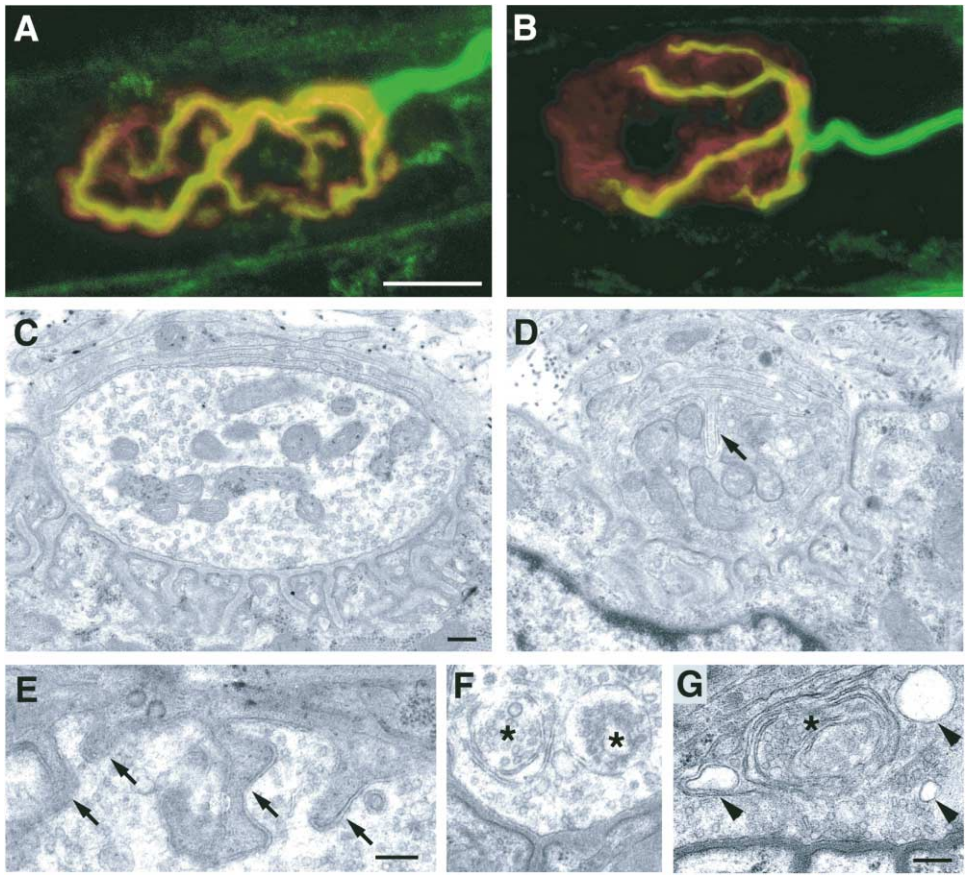

Figure 3. Light and Electron Microscopy of Neuromuscular Junctions from Wild-Type and CSPα KO Mice

(A and B) Confocal images of neuromuscular junctions (NMJs) from wild-type (A) and CSPα KO mice (B) double labeled with rhodamine-tagged α-bungarotoxin (red) and antibodies to neurofilaments and SV2 (green). (C–G) Electronmicrographs of NMJs from wild-type (C) and CSP KO mice (D–G) to illustrate morphological changes caused by the deletion of CSPα (see Table 1 for a quantitation of changes). Arrows in panels (D) and (E) identify Schwann cell intrusions, asterisks in panels (F) and (G) indicate multilamellar bodies, and arrowheads in panel (G) indicate vacuoles. (A)–(F) are from P23 animals; (G) is from a P17 animal (calibration bars: [A], 10 μm; [C], [E], and [G], 0.25 μm; [B], [D], and [F] are the same magnification as [A], [C], and [E], respectively).

processes extend between the presynaptic membrane and the synaptic cleft and ensheath the nerve terminal. In the CSPα mutants, in contrast, the terminal is indented rather than wrapped, and it is the "back side" of the terminal rather than the presynaptic face that is affected.

To ask whether the defects observed in CSPα KO mice were age dependent, we determined the incidence of abnormalities in the ultrastructure of NMJs at P7, P14, and P35 (Table 1). Defects were evident at all ages examined but were less striking at P7 than at later

Table 1. Ultrastructural Analysis of Neuromuscular Junctions in CSPα KO Mice

Age	Genotype	n	Folds/Profile	Active Zones/Profile	% with Schwann Cell Protrusions	% with Vacuole	% with Multilamellar Bodies
P7	+/+	26	1.1	1.4	0.0	42.3	7.7
	−/−	40	1.2	1.4	7.5	22.5	17.5
P14	+/+	44	5.5	1.6	4.5	9.5	4.8
	−/−	38	4.7	1.6	21.1**	28.9**	28.9**
P23	+/+	35	5.0	1.4	5.7	2.9	2.9
	−/−	45	5.7	1.0	44.4**	24.4**	22.2**
P35	+/+	33	6.6	2.2	6.1	3.0	9.1
	−/−	29	6.0	1.2*	31.0**	27.6**	24.1**

NMJs were examined by electronmicroscopy as described (Patton et al., 2001; see also Figure 3). "N" is the number of NMJ profiles counted, and "folds" refers to "junctional folds," membrane invaginations into muscle fibers directly across from the presynaptic active zone. Data are from two to three mice per age per genotype. Asterisks indicate significant differences ($p < 0.05$) between mutants and age-matched littermate controls (*, unpaired t test; **, contingency table analysis).

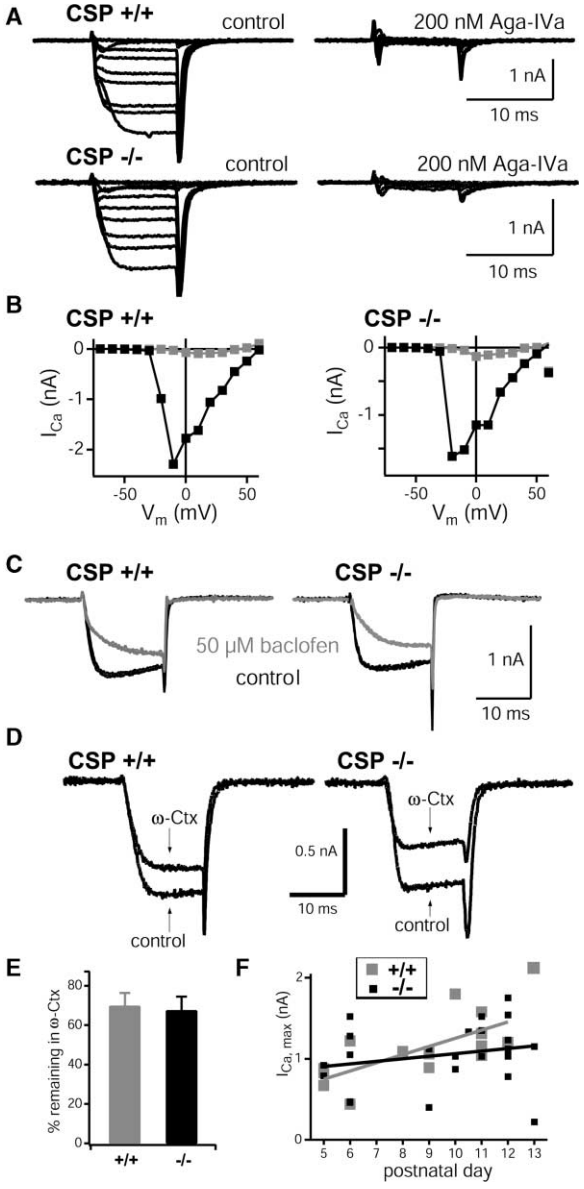

Figure 4. Presynaptic Ca^{2+} Currents at the Calyx of Held from Wild-Type and CSPα KO Mice

(A) Voltage-gated Ca^{2+} currents in Calyx terminals from wild-type (top) and CSPα KO mice (bottom) at P9–P13. Ca^{2+} currents were measured in response to depolarizations between -70 and $+60$ mV in the absence (left traces) or presence (right traces) of agatoxin-IVa (Aga-IVa; 0.2 μM), a specific P/Q-type Ca^{2+} channel blocker.

(B) Current-voltage (I/V) relations obtained from the experiments shown in (A). Black and gray symbols represent values recorded in the absence and presence of Aga-IVa, respectively.

(C) Voltage-gated Ca^{2+} currents recorded in response to three consecutive step depolarizations to 0 mV in the absence (black traces) or presence of the $GABA_B$ receptor agonist baclofen (50 μM; gray traces), which slows Ca^{2+} current activation and reduces peak Ca^{2+} current amplitudes in wild-type (left panel) and CSPα KO mice (right panel).

(D) Whole-cell recordings of presynaptic Ca^{2+} currents in response to step depolarizations to -10 mV, measured in Calyces of Held at P5–P6. Recordings were obtained before and after addition of the N-type-specific Ca^{2+} channel blocker ω-conotoxin GVIA (3 μM).

(E) Average blocking efficiency of 3 μM ω-conotoxin GVIA, expressed in percent of remaining Ca^{2+} current (n = 5 wild-type and n = 3 cells CSPα KO mice).

(F) Plot of the maximal Ca^{2+} current amplitude as a function of postnatal development between P5 and P13. Each data point represents the Ca^{2+} current measured at the peak of the I/V relation for a single cell (gray symbols, wild-type; black symbols, KO cells). Both data sets were fitted by linear regression (indicated by straight lines), revealing a slight developmental increase of Ca^{2+} current amplitudes.

stages. For example, the fraction of synapses with invaginated Schwann cell processes in the nerve terminal increased 300% between P7 and P14. In addition, the fraction of nerve terminals in CSPα KO mice with multilamellar bodies increased $\sim$50% between P7 and P14, despite the fact that more control terminals bore such bodies (and vacuoles) at P7 than at P14 (Table 1). Thus, the synaptic defects resulting from lack of CSPα are progressive during early postnatal life, suggesting that these defects are responsible, at least in part, for the sensorimotor impairments (Figure 2).

Ca^{2+} Channel Function in CSPα KO Mice

The initially normal function but subsequent progressive impairment of NMJs in CSPα KO mice are most consistent with the chaperone hypothesis of CSP function (see Introduction). However, these findings could potentially also be explained by a secondary effect of a role of CSPα in controlling presynaptic voltage-gated Ca^{2+} channels or in mediating a step in Ca^{2+}-triggered exocytosis. To distinguish more definitively between the three hypotheses of CSP function (Ca^{2+} channel activity, Ca^{2+}-triggered exocytosis, or chaperone; see Introduction), we examined Ca^{2+} channel function and synaptic transmission at the Calyx of Held synapse in the medial nucleus of the trapezoid body (MNTB). This synapse is uniquely suitable for precise measurements of Ca^{2+} currents and neurotransmitter release (Borst and Sakmann, 1996) and thus allows a direct test of the role of CSPα in these processes.

We first investigated presynaptic Ca^{2+} channel function in CSPα KO mice but failed to detect significant changes. We observed a similar activation time course and voltage dependence of Ca^{2+} currents in CSPα KO and control mice (Figure 4A) and similar current/voltage relationships of Ca^{2+} currents (Figure 4B). At P9–P12, when these measurements were performed, $>$85% of the presynaptic Ca^{2+} current at the Calyx synapse is mediated by Aga-IVa-sensitive, P/Q-type Ca^{2+} channels (Takahashi et al., 1996). Consistent with this finding, Aga-IVa toxin (0.2 μM) inhibited the majority of the Ca^{2+} currents in wild-type and KO synapses (Figure 4A). The degree of inhibition was indistinguishable between control and CSP-deficient synapses (wild-type, 93.4% $\pm$ 6.6%; KO, 92.1% $\pm$ 4.2% inhibition; n = 3 cells each).

It was proposed that CSPα regulates G protein modulation of Ca^{2+} channels (Magga et al., 2000). We therefore examined whether the coupling of a G protein-coupled receptor to voltage-gated Ca^{2+} channels might be impaired in CSPα KO mice. The Calyx of Held expresses presynaptic $GABA_B$ receptors whose activation causes a characteristic slowing of Ca^{2+} channel opening and a reduction of Ca^{2+} current amplitude (Takahashi et al., 1998; Isaacson, 1998). Figure 4C illustrates the effect

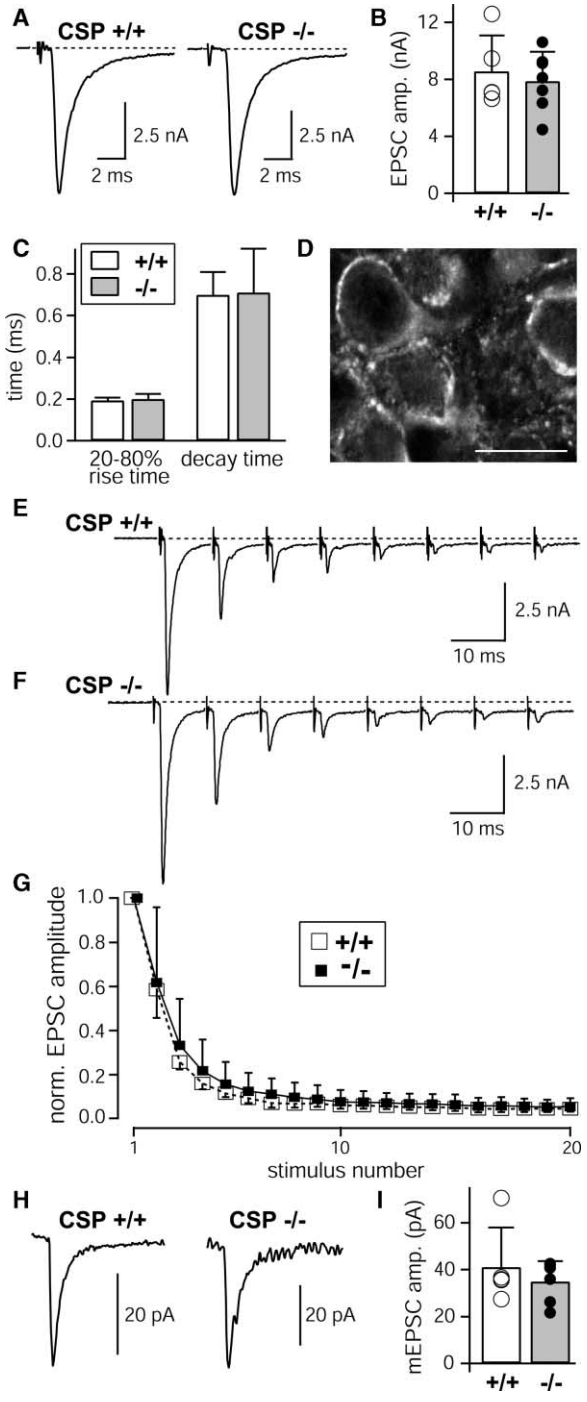

Figure 5. Synaptic Transmission at the Calyx of Held in Wild-Type and CSPα KO mice at P9–P11

(A) Representative traces from whole-cell recordings of excitatory postsynaptic currents (EPSCs) in MNTB principal neurons from wild-type or CSPα KO mice elicited by afferent fiber stimulation.

(B) Average EPSC amplitudes in cells from wild-type and CSPα KO mice (n = 5 and 7, respectively). Each point represents the average first EPSC amplitude of individual neurons recorded during four to eight successive 100 Hz stimulus trains (0.2 s) separated by 40–50 s. Bars show means ± SDs of the averages for each group.

(C) Mean 20%–80% rise times and mean decay time constants of EPSCs. The EPSC decay could be fitted with a double-exponential function; the plot shows the fast decay time constant that accounted for ~80% of the amplitude in wild-type and CSPα KO cells.

(D) Confocal image of a brainstem section from a wild-type mouse at P12 labeled with anti-CSPα antibodies. Ring-like Calyx synapses adjacent to the somata of the MNTB principal cells and smaller, noncalyceal synapses are clearly visible (calibration bar, 20 μm). Parallel studies of CSPα KO slices showed that the staining was abolished (data not shown).

(E and F) Representative traces of EPSCs during a 100 Hz stimulus train.

(G) Time course of the depression of EPSCs during 100 Hz stimulus trains. EPSC amplitudes during five to eight successive stimulus trains were normalized to the first response and averaged for all cells (means ± SDs; n = 5 wild-type/7 KO cells).

(H) Average mEPSC traces for a wild-type cell (left panel, average of n = 634 mEPSCs) and for a CSPα KO cell (right panel, average of n = 28 mEPSCs). Note the similar mEPSC amplitudes and kinetics for both genotypes.

(I) mEPSC amplitudes in wild-type and CSPα KO mice (n = 5 and 7, respectively). Each point represents the average mEPSC amplitude for a given cell, taken as the mean of the mEPSC amplitude distribution.

of 50 μM baclofen, a saturating concentration of this selective $GABA_B$ receptor agonist, on presynaptic voltage-gated Ca^{2+} currents recorded during a 15 ms step to 0 mV. We found no difference between wild-type and CSPα KO mice (n = 3 cells each) in the responses of Ca^{2+} currents to baclofen (Figure 4C), indicating that the G protein-mediated coupling of $GABA_B$ receptors to P/Q-type Ca^{2+} channels, the predominant Ca^{2+} channel subtype at this developmental stage, is unchanged.

In calyces of the chick ciliary ganglion, whole-cell perfusion with recombinant CSPα increased the amplitude of presynaptic Ca^{2+} currents, suggesting that CSPα may recruit previously inactive Ca^{2+} channels (Chen et al., 2002). However, the presynaptic Ca^{2+} currents in the calyces of the ciliary ganglion are predominantly N-type (Stanley, 1991; Yawo and Chuhma, 1994), while N-type Ca^{2+} channels account only for a minority of Ca^{2+} channels in the Calyx of Held (Wu et al., 1999). To specifically monitor presynaptic N-type Ca^{2+} currents in CSPα KO mice, we examined calyces from younger mice in which the contribution of N-type Ca^{2+} channels to the overall Ca^{2+} current is larger (~30%; Iwasaki et al., 2000; Wu et al., 1999). We asked whether the ω-conotoxin-sensitive component of the presynaptic Ca^{2+} current was reduced in young (P5–P6) CSPα KO mice, as would be expected if functional N-type Ca^{2+} channels were recruited by CSPα (Chen et al., 2002). We applied 3 μM ω-conotoxin to slices and monitored presynaptic Ca^{2+} channels by voltage steps (to −10 mV, 15 ms) that were applied every 15 s (Figure 4D). Although the magnitude of the ω-conotoxin block varied between terminals, we again detected no significant difference between wild-type and CSPα KO mice in the average blocking effect (Figure 4E).

Finally, we searched for alterations in the peak Ca^{2+} currents in calyces of Held from CSPα KO versus wild-type littermate mice (Figure 4F) at ages between P5 and P13. In Figure 4F, each data point represents the maximal Ca^{2+} current amplitude for a given cell, taken from I-V relations as shown in Figure 4B. For both genotypes, we observed a slight developmental increase in peak Ca^{2+} current amplitude but detected no consistent difference between wild-type and KO cells. Two calyces

from CSPα KO animals exhibited small peak Ca^{2+} currents that were not found in the littermate wild-type controls (Figure 4F). However, since the remaining 23 KO calyces were indistinguishable from wild-type controls, the average peak Ca^{2+} currents were not significantly different between wild-type (1.14 ± 0.38 nA; n = 18) and CSPα KO mice (1.05 ± 0.38 nA; n = 25). Together, these data show that CSPα is not essential for presynaptic Ca^{2+} channel function.

Synaptic Transmission in CSPα KO Mice

We next tested the second hypothesis, namely, that CSP is directly involved in exocytosis, by measuring synaptic transmission in the Calyx of Held synapse from wild-type and KO mice at P9–P11. Using afferent fiber stimulation in brainstem slices, we applied 20 stimuli at 100 Hz and employed postsynaptic whole-cell recordings to monitor AMPA receptor-mediated excitatory postsynaptic currents (EPSCs).

We first examined the initial synaptic responses in the stimulus trains (Figures 5A). The shapes and amplitudes of the EPSCs were similar in wild-type and KO littermate mice ($CSP^{+/+}$, 8.6 ± 2.5 nA; $CSP^{-/-}$, 7.88 ± 2.05 nA; Figure 5B), and the 20%–80% rise times of the EPSCs were nearly identical (Figure 5C). To assess the decay of the EPSCs, we fitted the responses with a double-exponential function. The fast component accounted for ~80% of the EPSC amplitude and again was indistinguishable between wild-type and KO cells (Figure 5C). These data suggest that CSPα is not essential for release at P9–P11. To confirm that CSPα is in fact expressed at this stage in the Calyx synapse, we performed immunofluorescence analyses, which demonstrated that CSPα could be reliably detected in Calyx terminals in wild-type but not KO mice (Figure 5D and data not shown).

We then asked whether deletion of CSPα alters synaptic responses during stimulus trains (Figures 5E–5G). We observed a marked short-term depression during 100 Hz stimulation (Borst et al., 1995; von Gersdorff et al., 1997; Wang and Kaczmarek, 1998) without significant differences between wild-type and CSPα KO cells. To analyze this quantitatively, we constructed for each cell a mean depression curve from four to eight successive 100 Hz stimulus trains. The depression curves were normalized and averaged for all wild-type and KO cells (Figure 5G). The relative amplitude of the second compared to the first EPSC ($CSP^{+/+}$, 59% ± 13%; $CSP^{-/-}$, 62% ± 34%) and the near steady-state depression at the end of the 100 Hz trains ($CSP^{+/+}$, 4.7% ± 1.5%; $CSP^{-/-}$, 5.6% ± 3.7% of initial EPSC amplitude) were similar. However, synaptic responses in the CSPα KO were more heterogeneous than in wild-type mice, as reflected by their larger error bars (Figure 5G).

Finally, to analyze the quantal properties of transmitter release, we sampled spontaneously occurring miniature EPSCs (mEPSCs) in the recording intervals between evoked EPSCs. We detected no significant difference between wild-type and CSPα KO cells in the average shape (Figures 5H) or mean amplitude of the mEPSC (Figure 5I). Together with the unchanged EPSC parameters (Figures 5A–5C), these results indicate that, at P9–P11, the amount and kinetics of quantal release in response to afferent fiber stimulation are not altered in CSPα KO mice.

Kinetics of Release in CSPα KO Neurons

To search for more subtle changes in exocytosis in the CSPα KO mice, we next analyzed the slow and the fast components of transmitter release using paired pre- and postsynaptic voltage-clamp recordings. Recordings were performed in the presence of extracellular cyclothiazide (100 μM) and kynurenic acid (1 mM) to reduce desensitization and saturation of postsynaptic AMPA receptor responses. Release was triggered by a presynaptic voltage-clamp protocol in which steps to +80 mV are interrupted by brief excursions of 0.8 and 2 ms to 0 mV (Neher and Sakaba, 2001). This protocol measures the effectiveness of a defined period of Ca^{2+} influx in inducing transmitter release, monitored via the EPSC (Figure 6A).

The kinetic parameters of the EPSCs were similar between CSPα KO mice and wild-type littermates at P9–P11 (Figure 6A). EPSCs monitored in these recordings decayed slightly slower than EPSCs recorded after fiber stimulation (Figure 5), presumably because the cyclothiazide delayed receptor desensitization and deactivation. The average amplitudes of the EPSCs during the first and second stimulus and of the summed EPSCs were not significantly different between wild-type and KO cells (Figure 6D). This indicates that transmitter release in response to brief Ca^{2+} influx was not altered in CSPα KO mice.

We then analyzed the kinetics of the rapidly and slowly releasable pools of vesicles after prolonged (~50 ms) presynaptic voltage-clamp depolarization to 0 mV (Sakaba and Neher, 2001). We monitored EPSCs in Calyx terminals that were depolarized to +80 mV for 4 ms and then held at 0 mV for either 4 ms or 50 ms (Figure 6B). The short 4 ms stimulus induced a fast burst of transmitter release, while the longer 50 ms stimulus induced a second slower phase in addition to the initial fast burst (Sakaba and Neher, 2001). We derived the cumulative transmitter release rates for both stimuli by deconvolution of the EPSCs (Figure 6C) and fitted the time course of cumulative release with double-exponential functions. We detected no consistent difference in the time constants of both phases of transmitter release between CSPα KO and wild-type mice (Figure 6E). Thus, the kinetics of transmitter release were unchanged in CSPα KO mice, suggesting that the coupling of Ca^{2+} channels to vesicle fusion and the Ca^{2+} sensitivity of vesicle fusion were not significantly altered.

Progressive Loss of Synaptic Function at the Calyx of Held

The Ca^{2+} current and EPSC recordings at the Calyx synapse effectively rule out the first two hypotheses about CSP function—an essential role in controlling Ca^{2+} channel activity or exocytosis—but raise the question whether CSPα has any function in the Calyx. Since at the NMJ the CSPα KO mice exhibited an age-dependent progressive neurodegenerative phenotype that was indicative of a chaperone function (see Figures 1–3), we asked whether synaptic transmission at the Calyx of Held also becomes abnormal later in development, consistent with such a function. To test this, we examined synaptic transmission in Calyx synapses using afferent fiber stimulation at P20–P23 (Figure 7) with exactly the same protocol as described above for mice at P9–

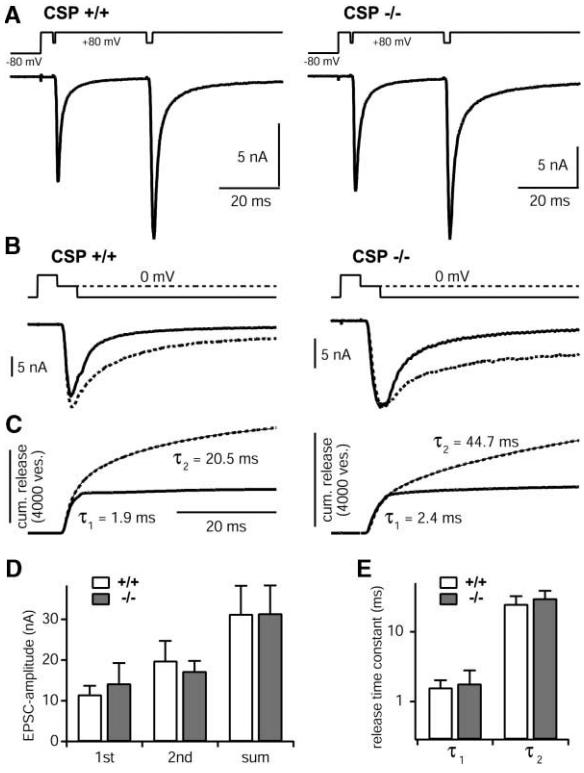

Figure 6. Paired Recordings of Synaptic Responses at the Calyx of Held from Mice at P9–P12

(A) EPSCs elicited by short periods of presynaptic Ca^{2+} influx. The presynaptic voltage-clamp protocol used (schematically diagrammed above the electrophysiological traces) depolarizes the cells to +80 mV (at which point the driving force for Ca^{2+} influx is strongly reduced). Ca^{2+} influx is then induced by returning the membrane potential from +80 mV to 0 mV for 0.8 ms (first stimulus) and 2 ms (second stimulus).

(B) EPSCs elicited with longer periods of presynaptic Ca^{2+} influx. In this protocol (shown schematically above the traces), the membrane potential is raised to +80 mV for 4 ms, Ca^{2+} influx is then induced by repolarization to 0 mV for 4 ms or for 50 ms, and finally Ca^{2+} channels are closed by repolarization to −80 mV.

(C) Integrated transmitter release rates obtained by deconvolution of the EPSCs shown in panel (B) (straight and dashed lines = 4 and 50 ms stimulations, respectively). Release rates in response to 50 ms depolarizations were fitted with a double-exponential function, resulting in estimated time constants of a fast and a slower release component.

(D) Average EPSC amplitudes measured with the protocol shown in panel (A). Bars represent EPSC amplitudes in response to the first (0.8 ms) and second (2 ms) repolarizations to 0 mV and the summed EPSC amplitudes in response to both stimuli.

(E) Average time constants of pool depletion estimated in the experiments shown in (B) (for panels [D] and [E], $CSP^{+/+}$, n = 4; $CSP^{-/-}$, n = 7 cell pairs).

P11 (Figure 5). As summarized below, we observed dramatic changes in CSPα KO mice at P20–P23 that are consistent with a functional deterioration of synaptic transmission.

In wild-type mice, the initial EPSC amplitude was larger at P20–P23 (13.3 ± 3.1 nA; [n = 5]) than at P9–P11 (8.6 ± 2.5 nA). This increase reflects the normal maturation of the Calyx synapse (Taschenberger and von Gersdorff, 2000; Iwasaki and Takahashi 2001; Joshi and Wang, 2002). In CSPα KO mice, however, the average initial EPSC amplitude was smaller at P20–P23 (5.62 ± 5.43 nA [n = 5]; Figure 7B) than at P9–P11 (7.88 ± 2.05 nA). Thus, at P20–P23, the average EPSC amplitude in KO cells is ~2-fold lower than in wild-type cells ($p = 0.016$ in a one-tailed, two-sample unequal variance t test), whereas at P9–P11 there was no statistically significant difference between KO and wild-type cells. In these experiments, the average EPSC amplitudes were calculated from the highly reproducible mean EPSCs of individually analyzed cells. These mean ESPCs were variable between mutant cells, as reflected in the large standard deviation of the average shown above, whereas the mean EPSCs were much less variable between wild-type cells (Figure 7B). Although we occasionally observed EPSCs in the range of 5–14 nA in KO cells, some cells produced an initial EPSC amplitude of only ~1 nA (1.03 and 0.98 nA; n = 2 cells). In fact, we probably overestimated the average EPSC amplitude in the CSPα KO mice at P20–P23, because we used extracellular recordings of pre- and postsynaptic action potentials to preselect neurons in which the Calyx input could be stimulated successfully by afferent fiber stimulation (Borst et al., 1995). Normally, our success rate in finding a neuron with pre- and postsynaptic action potentials is 10%–20% (Meyer et al., 2001). However, in CSPα KO mice at P20–P23, we recorded action potentials only in <5% of postsynaptic cells, indicating that many calyceal EPSCs were too small to reliably induce a postsynaptic action potential, a result that is consistent with the loss of presynaptic nerve terminals seen morphologically (see below).

In wild-type mice, the rise times were shorter, and the fast decay component of the EPSC—which now accounted for >95% of the total EPSC—was accelerated at P20–P23 compared to P9–P11 (Figures 7A–7C). In contrast, the EPSCs in CSPα KO mice did not rise and decay as smoothly but often exhibited irregularities (Figure 7A, right panel). The average EPSC rise and decay times were approximately two times slower in CSPα KO mice than in wild-type littermate controls (Figure 7C). This together with the fact that the kinetics of mEPSCs were unchanged (see below; Figure 7H) indicates that transmitter release was more asynchronous in the CSPα KO mice.

Furthermore, at P20–P23, CSPα KO mice exhibited dramatic changes in short-term plasticity. Wild-type synapses experienced less depression of EPSCs during 100 Hz stimulus trains at P20–P23 than at P9–P12 (e.g., compare Figure 5E with Figure 7D). In CSPα KO synapses, however, we often observed facilitation instead of depression (Figures 7E and 7F). Again, responses were heterogeneous (see large error bars in the summary graph of Figure 7G) and occasionally obscured by noncalyceal inputs (Figure 7E). The principal neurons of the MNTB receive a second synaptic glutamatergic input in addition to the dominant Calyx input. This second input generates a delayed EPSC of a smaller amplitude (Forsythe and Barnes-Davies, 1993; see Figure 7D, arrows). In some KO cells, the small initial EPSC amplitude made it difficult to distinguish the calyceal input from noncalyceal excitatory inputs. In order to differentiate between calyceal and noncalyceal EPSCs, we therefore recorded EPSCs at varying stimulation intensities. In all cells included in the final data set, the calyceal input was clearly separated from a smaller, presumably noncalyceal input on the basis of their different stimula-

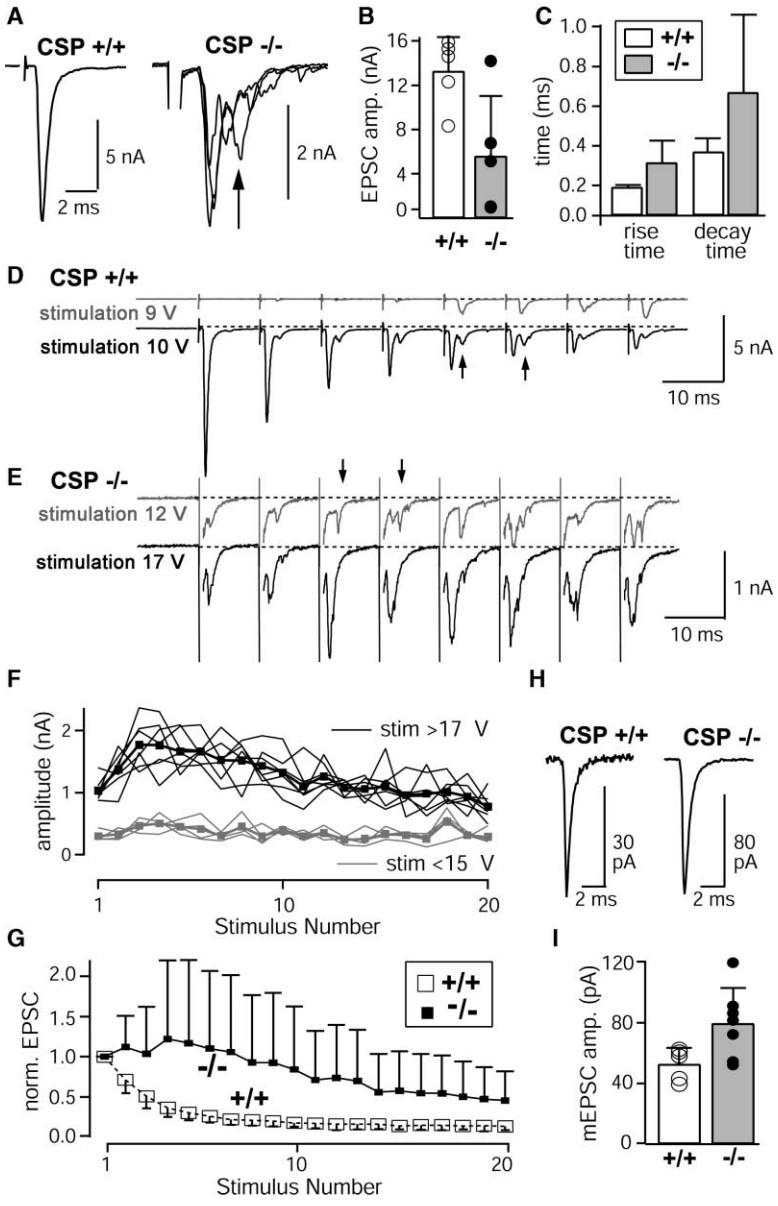

Figure 7. Reduction and Desynchronization of Synaptic Transmission in the Calyx of Held of CSPα KO Mice at P20–P23

(A) Representative EPSCs elicited by afferent fiber stimulation. The second EPSC peak that appeared with a longer latency in the CSPα KO traces (arrow) is probably due to a noncalyceal input.

(B) Average EPSC amplitudes in cells from wild-type and CSPα KO mice (n = 5 for both). Each point represents the average first EPSC amplitude of individual neurons recorded during four to eight successive 100 Hz stimulus trains (0.2 s separated by 40–50 s). Bars show means ± SDs for each group.

(C) Mean 20%–80% rise times and decay time constants of EPSCs from wild-type (white bars) and CSPα KO cells (gray bars).

(D) Wild-type synaptic responses to 100 Hz afferent fiber stimulation. With a stimulus intensity of 9 V, a noncalyceal EPSC with small amplitudes was observed (gray trace). Increasing the stimulus strength to 10 V or higher induced a large calyceal EPSC (black trace). The noncalyceal EPSC remains visible (see arrows) because it has a longer latency than the calyceal EPSC.

(E) A similar experiment in a CSPα KO cell. Systematically varying the stimulus intensity between 10 to 25 V revealed two distinct excitatory inputs with clearly separable amplitudes.

(F) Plot of EPSC amplitudes at stimulation intensities below 15 V (gray traces) or above 17 V (black traces) for the cell shown in (E). Two excitatory inputs are separable based on their differential stimulation thresholds. The larger, calyceal input had a threshold of 17 V and an initial amplitude of ~1 nA, which facilitated to ~1.8 nA during the fourth stimulus.

(G) Normalized average synaptic responses recorded during 100 Hz stimulus trains from wild-type (open symbols) and CSPα KO neurons (closed symbols). Note the large variability among KO responses reflected in the error bars representing SDs.

(H) Average mEPSC traces for a wild-type (average of n = 101 mEPSC traces) and a CSPα KO cell (average of n = 94 traces).

(I) Average mEPSC amplitude for individual cells (open and closed symbols for wild-type and CSPα KO cells, respectively; bars show means ± SDs). The mEPSC amplitude in CSPα KO cells was significantly increased (p = 0.025; two-tailed, unequal variance t test).

tion thresholds. In the KO cell shown in Figure 7E, for example, stimulation below 15 V activated a small, noncalyceal input, whereas stimulation above 17 V activated EPSCs with clearly larger amplitudes (compare gray and black lines in Figure 7F) that likely represent transmitter release from the Calyx of Held.

Finally, we examined mEPSCs at P20–P23 (Figures 7H and 7I). The mEPSC rise and decay kinetics were similar for wild-type and KO cells (average decay time constants: $CSP^{+/+}$, 230 ± 57 μs, n = 5; $CSP^{-/-}$, 277 ± 130 μs, n = 7), but the average mEPSC amplitude was larger in CSPα KO mice (Figure 7I; $CSP^{+/+}$, 53 ± 11 pA, n = 5; $CSP^{-/-}$, 80 ± 23 pA, n = 7; p = 0.025). Among others, this increase in mEPSC amplitude could result from a presynaptic increase in glutamate loading (Ishikawa et al., 2002) or an enhanced density of postsynaptic AMPA receptors. The increased mEPSC amplitude in CSPα KO cells might be a mechanism by which the Calyx synapse partially compensates for the decrease in presynaptic transmitter release and indicates that the release probability may be decreased by a larger degree than a simple comparison of the evoked EPSC amplitudes (Figure 7B) would suggest.

Presynaptic Degeneration in the Calyx of Held from CSPα KO Mice

In the NMJ of CSPα KO mice, the decline in physiological properties (Figure 2) is paralleled by a morphological degeneration (Figure 3 and Table 1). To determine whether the age-dependent functional impairment of Calyx terminals (Figure 7) also correlates with a morphological change, we examined Calyx synapses in wild-type and CSPα KO mice at P25 by electron microscopy (Figure 8).

CSPα KO mice exhibited major changes in synapse structure consistent with a presynaptic degenerative process. In CSPα KO mice, the cell bodies of principal

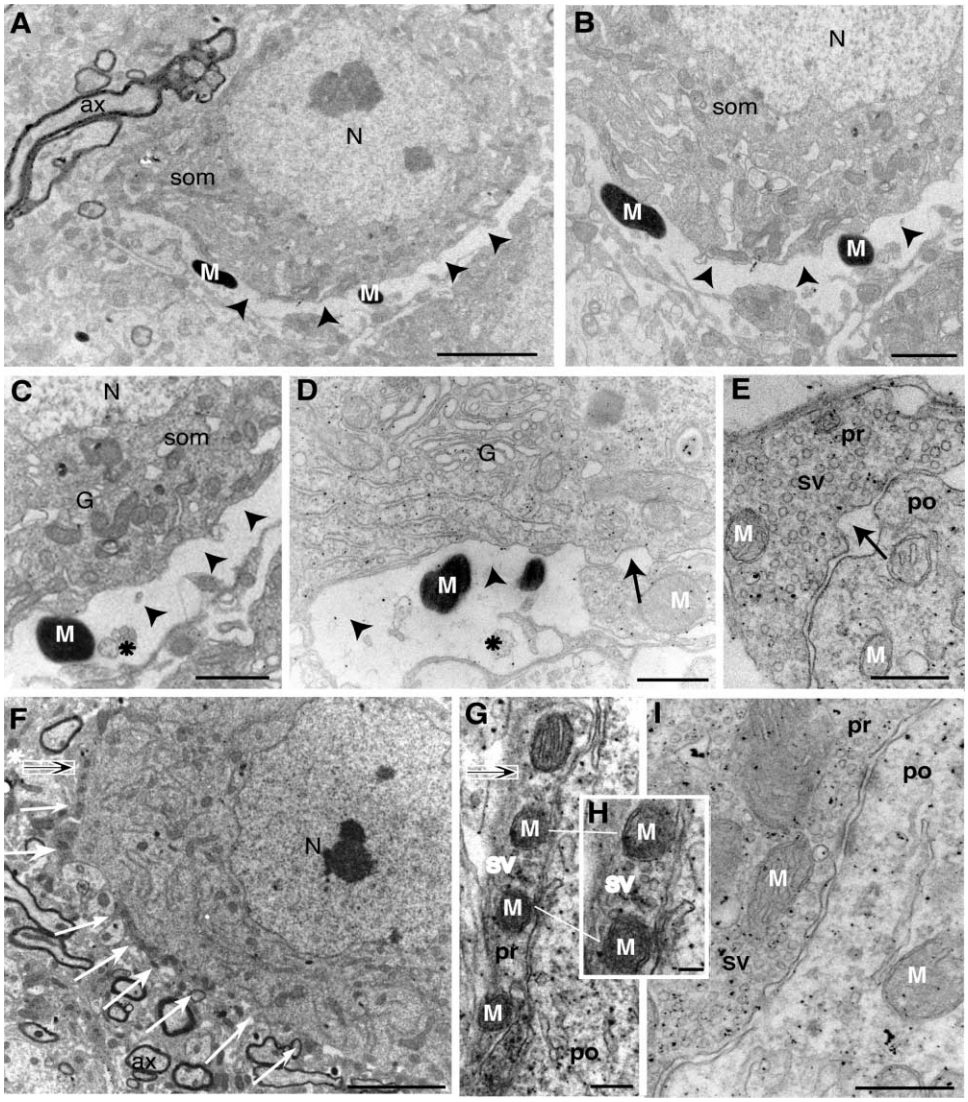

Figure 8. Degenerative Changes of Presynaptic Calyx Terminals in the MNTB from CSPα KO Mice

Images show electronmicrographs of Calyx synapses from CSPα KO (A–E) or wild-type mice (F–I). (A and F) Low-magnification electron micrographs of Calyx synapses in the MNTB from KO and wild-type animals, respectively. In (A), the electron-lucent spaces in the KO mice (arrowheads) probably correspond to degenerated presynaptic terminals because of their typical location surrounding postsynaptic cells. (B–D) Degenerated presynaptic terminals (arrowheads) at higher magnification; note the characteristic electron-dense degenerated mitochondria ("M"). In some cases, remnants of vesicles are visible in the degenerated terminals (asterisks in [C] and [D]). Arrows in (D) and (E) indicate widened synaptic clefts in CSPα KO animals which are also present in wild-type animals (data not shown; Lenn and Reese, 1966). Not all Calyx terminals in the MNTB of CSP KO mice were degenerated, but some had a wild-type appearance (E). Abbreviations: ax, axon; som, soma of a postsynaptic principal cell; N, nucleus; M, mitochondrion; SV, synaptic vesicle; pr, presynaptic terminal; po, postsynaptic principal cell; G, Golgi apparatus. Scale bars, 5 μm (A); 2.5 μm (B); 1.5 μm (C); 1 μm (D); 1 μm (E); 5 μm (F); 300 nm (G); 120 nm (H); 1 μm (I).

MNTB neurons were often surrounded by conspicuous 1–2 μm wide electron-lucent areas (Figure 8A, arrowheads). These areas contained black, electron-dense particles that were tentatively identified as degenerated mitochondria due to their size, shape, and distribution (Figures 8A–8D). The degenerative changes in CSPα KO mice were heterogeneous: higher magnifications showed that the electron-lucent spaces were adjacent to normal-looking presynaptic terminals (Figures 8D and 8E) and probably fill the spaces previously occupied by presynaptic terminals. A widened synaptic cleft—which is also observed in some normal calyces of Held (Lenn and Reese 1966)—is continuous with the electron-lucent areas in the CSPα KO mice (Figure 8D, arrow and arrowheads). In some cases, electron-lucent areas contained aggregates of agglutinated presynaptic vesicles (Figures 8C and 8D, asterisks), suggesting that degenerated presynaptic terminals of the Calyx of Held are continuous with the extracellular space. In contrast, in wild-type sections, the principal cells are surrounded by presynaptic terminals whose cytoplasm is characterized by strings of mitochondria (Figure 8F, white arrows; Taschenberger et al., 2002; Sätzler et al., 2002) and at higher magnification are shown to contain presynaptic vesicles, active zones, and pre- and postsynaptic densities (Figures 8G–8I). Quantifications showed that the area

of postsynaptic cells that is in direct contact with a presynaptic nerve terminal is much smaller in CSPα KO mice (15.7% ± 8.3% of the cell surface; n = 25) than in wild-type controls (48.0% ± 12.5%; n = 25). The postsynaptic cells of KO mice have a normal appearance but are smaller than wild-type controls (average circumference: wt, 54.3 ± 8.1 μm; KO, 42.6 ± 5.6 μm; longest and shortest diameters: wt, 19.1 ± 2.8 and 12.9 ± 2.1 μm; KO, 14.7 ± 2.1 and 10.3 ± 2.3 μm, respectively; n = 50 of both genotypes).

Discussion

CSP is an abundant synaptic vesicle protein that is composed of an N-terminal J domain and a C-terminal string of cysteine residues (Zinsmaier et al., 1990). Based on genetic experiments in *Drosophila*, transfection studies in vertebrates, and biochemical observations with *Drosophila* CSP and rat CSPα, three principal hypotheses of CSP function emerged. The first two hypotheses postulate an essential role for CSP in the assembly, activation, or regulation of Ca^{2+} channels (Gundersen and Umbach, 1992; Leveque et al., 1998; Ranjan et al., 1998; Umbach et al., 1998; Magga et al., 2000; Chen et al., 2002) or in exocytosis, possibly by binding to SNARE proteins or to synaptotagmin 1 (Umbach et al., 1994; Zinsmaier et al., 1994; Dawson-Scully et al., 2000; Graham and Burgoyne, 2000; Bronk et al., 2001; Evans and Morgan, 2002). The third hypothesis posits that CSP acts as a presynaptic chaperone (Braun et al., 1996; Chamberlain and Burgoyne, 1997; Tobaben et al., 2001). In the present study, we tested these three hypotheses using KO mice that lack CSPα (the only brain isoform of vertebrate CSP; see the Supplemental Data at http://www.neuron.org/cgi/content/full/42/2/237/DC1). In these experiments, we studied two independent synapses (the NMJ and the Calyx of Held) and employed ultrastructural and electrophysiological analyses in both preparations to determine the role of CSPα. Our data describe a severe, age-dependent phenotype in CSPα KO mice that can be summarized as follows:

(1) In the first 2 postnatal weeks, CSPα KO mice exhibited no overt impairments. However, after P14, the KO mice stopped gaining weight, and after P21, they started dying because of a progressive neurological disorder (Figures 1 and 2). This time course is typical for a degenerative process which becomes apparent after a lag period. In contrast, mutations that impair synapse function directly typically cause a burst of mortality around birth (e.g., see SV2 KO mice; Janz et al., 1999).

(2) CSPα KO mice exhibited severe age-dependent impairments in all neurological parameters examined (Figure 2). Some impairments (e.g., in maintaining balance; Figure 2C) were apparent before P15 when the CSPα KO mice stopped gaining weight, whereas other defects became progressively more severe after P25 (e.g., the defect in righting; see Figure 2D).

(3) In a direct test of the hypothesis that CSP is required for Ca^{2+} channel function, we measured presynaptic Ca^{2+} currents in Calyx terminals from CSPα KO mice at P5–P13. We failed to uncover any detectable impairment (Figure 4). Neither the amplitude nor the regulation of Ca^{2+} currents was altered, demonstrating that CSPα is not required for Ca^{2+} channel function.

(4) To probe for a role for CSPα in exocytosis, we monitored the magnitude and kinetics of neurotransmitter release in the calyx and examined myographic responses in the NMJ. In young CSPα KO mice, we detected no abnormalities, as reflected in the normal CMAP amplitude at the NMJ (Figure 2F) and the normal EPSC kinetics and amplitudes at the Calyx of Held synapse (Figures 5A and 5C). Moreover, in the Calyx synapse at P9–P11, CSPα-deficient synapses exhibited the same time course of synaptic depression during repetitive stimulation as wild-type controls (Figure 5G). Together, these findings rule out a major direct role for CSPα in the release machinery.

(5) Consistent with their neurological impairments, we observed in CSPα KO mice age-dependent functional and morphological changes in the NMJs (Figures 2 and 3 and Table 1). Functionally, the CMAP amplitudes decreased (Figure 2F), and synaptic responses displayed severe use-dependent depression (Figure 2G). Morphologically, NMJs in older KO mice exhibited prominent abnormalities such as persistent vacuoles, proliferation of multilamellar bodies, and protrusion of Schwann cell fingers into the neuromuscular nerve terminal. The NMJ abnormalities could explain the loss of muscle strength in CSPα KO mice and are consistent with a requirement for CSPα in maintaining nerve terminal membrane traffic.

(6) In the Calyx synapse, we also observed an age-dependent deterioration of synaptic function in CSPα KO mice (Figures 7A and 7B). Direct comparison of synaptic transmission at the Calyx at P9–P11 (Figure 5) and at P20–P23 (Figure 7) showed that the average EPSC size decreased ~2-fold in KO mice and that the release kinetics became highly abnormal. At P20–P23, synaptic responses exhibited a large degree of heterogeneity between cells, ranging from apparently normally responding cells to cells in which synaptic responses had become extremely small.

(7) Finally, ultrastructural examination of the Calyx by electron microscopy revealed a severe degeneration of nerve terminals in CSPα KO mice at P25 (Figure 8). The percentage of the postsynaptic cell surface covered by nerve terminals decreased by more than 3-fold. Neurodegeneration was heterogeneous in that normal-looking nerve terminals (which might correspond to the almost normal synaptic transmission observed in some cells in the electrophysiological measurements in CSPα KO mice at P20–P23) were often adjacent to completely degenerated terminals.

Our data show that deletion of CSPα causes a progressive dysfunction of synapses that kills the KO mice. This dysfunction is not due to a discrete feature of presynaptic neurotransmitter release (e.g., impaired Ca^{2+} channel function) but appears to be caused by a use-dependent loss of nerve terminal integrity. At the NMJ, we observed morphological abnormalities immediately after birth, whereas in the Calyx, even sensitive tests detected no changes in transmitter release until the animals were 3 weeks of age. This suggests that different types of synapses degenerate at distinct rates, possibly in a use-dependent manner.

The phenotype of the CSPα KO mice is best explained by a discrete function for CSPα in maintaining the integrity of synapses in the face of use-dependent stresses. According to this explanation, CSPα prevents neurode-

generation when the demands of normal function (continuous synaptic vesicle exo- and endocytosis) place a burden on the protein machinery involved. We thus propose that CSPα participates in a salvage process that recycles damaged components of the release machinery and that the previously characterized enzymatically active chaperone complex formed by CSPα with Hsc70 and SGT (Tobaben et al., 2001) mediates this salvage. In the absence of CSPα, components of the release machinery, such as SNARE proteins or Ca^{2+} channels, may become secondarily disabled, causing a defect in presynaptic function. It is possible that the salvage function of CSP involves an interaction of CSP with components of the release machinery, for example, as a repair complex when such components become disabled, which might explain some of the in vitro interactions observed for CSP (Nie et al., 1999; Evans and Morgan, 2002).

An alternative hypothesis to the chaperone function for CSP is that CSP does after all control Ca^{2+} channels or exocytosis but that this function is redundant in young mice with another protein which is developmentally downregulated, thereby leading to a phenotype in adult mice. According to this hypothesis, the neurodegenerative changes would be secondary to a specific loss of function. We believe this hypothesis is highly unlikely for several reasons. First, no protein closely related to CSPα is expressed in brain at significant levels as analyzed by GenBank searches and RNA measurements. Although mice contain two additional CSP genes, expression of these genes is not detectable in brain and is not upregulated in the CSPα KO (see the Supplemental Data at http://www.neuron.org/cgi/content/full/42/2/237/DC1), ruling out the possibility that redundancy between different CSP isoforms may obscure an otherwise more severe phenotype. Second, as assayed in a homogeneous population of synapses (the calyx terminals in the brainstem), the CSPα KO phenotype develops in a heterogeneous manner. In the KO mice, apparently normal nerve terminals are observed next to terminals that are completely degenerated (see Figure 8). Among more than ten synaptic loss-of-function mutants that have been analyzed (reviewed in Fernández-Chacón and Südhof, 1999; Südhof, 2004), none exhibit this kind of heterogeneity. Such heterogeneity is typical for a degenerative process but unexpected for a uniform loss-of-function event. Third, the physiological loss-of-function phenotype at the NMJ and the Calyx synapse did not precede the neurodegenerative changes observed morphologically but coincided with them or even followed them, suggestive of a primary neurodegenerative process. Fourth, loss of synaptic function does not usually lead to neurodegeneration. If one blocks synaptic function in muscle, for example, the morphological phenotype differs from that observed in the CSP KO mice, indicating that the morphological phenotype is not caused by a loss of synaptic transmission. Finally, the electrophysiological phenotype of the CSPα KO mice lacks a discrete electrophysiological signature, such as a selective loss of Ca^{2+} current or a discrete change in a release component, but instead consists of an age-dependent global change.

Our conclusions are at variance with conclusions derived in studies on CSP mutants in *Drosophila* (e.g., Ranjan et al., 1998; Umbach et al., 1998; Dawson-Scully et al., 2000), but the two data sets may be more compatible than is immediately apparent. CSP-deficient flies exhibit a temperature-sensitive phenotype, which is unexpected for a null mutant in a protein that has an essential function in vesicle exocytosis but fits well with a chaperone function. Moreover, *Drosophila* CSP genetically interacts with Hsc70 (Bronk et al., 2001), and both *Drosophila* NMJ and CSPα-deficient Calyx synapses exhibit desynchronized release (Heckmann et al., 1997, and Figure 7). The differences between our conclusions and those obtained with cells that contain overexpressed or microinjected CSPα (e.g., Magga et al., 2000; Graham and Burgoyne, 2000; Chen et al., 2002) are more difficult to explain. One possibility is that overexpressed CSPα may become dominant-negative because it is incompletely palmitoylated, remains partly soluble, and/or sequesters Hsc70 and SGT away from endogenous CSP. Another possibility is that the sheer overexpression of a heavily palmitoylated protein is deleterious to the cells. Independent of whether these two or other explanations are correct, the results illustrate the difficulties in overexpression studies to examine the function of a protein.

As a chaperone specialized for presynaptic terminals, interference with CSPα function could potentially be a mechanism of causing neurodegenerative diseases. For example, environmental toxins that inhibit CSPα function would probably cause an ascending paralysis. Although it is not excluded that such changes contribute to common neurodegenerative diseases, there is currently no direct support for this notion. Amyotrophic lateral sclerosis clinically resembles the phenotype of the CSPα KO mice, but the pathology of amyotrophic lateral sclerosis differs from that of the CSPα mutants. No evidence for a dysfunction of CSPα in Alzheimer's disease which severely affects synaptic function (Selkoe, 2002) has been reported but may have been overlooked because it has not been tested. Our results identify CSPα as a potential disease target that as an enzyme might be particularly sensitive to long-term changes (e.g., effects of a relatively small decrease in activity) and that may only be affected in the brain area that is the site of the disease. Future studies will have to explore whether CSPα is in fact affected in such a situation.

Experimental Procedures

Generation of CSPα KO Mice

Generation of CSPα KO mice was performed essentially as described (Rosahl et al., 1995; Janz et al., 1999) using SM1 embryonic stem cells cultured on irradiated STO cells. Mice were genotyped by PCR in a single tube reaction (Primer *A* = TGGTAGACTAACC TAACATGGCCG; Primer *B* = TTGGCCCACCAGCTGGAGAGTAC; Primer *C* (T676) = GAGCGCGCGCGGCGGAGTTGTTGAC; A versus B = ~1.2 kb wild-type product; B versus C = ~0.9 kb mutant product). Mice were maintained using standard mouse husbandry. For survival and weight curves, the mice were tagged immediately after birth and examined daily for almost 3 months.

Neurological Analyses

Neurological analyses were generally performed with a modified SHIRPA protocol (Rogers et al., 1997; http://www.mgu.har.mrc.ac.uk/mutabase/shirpa_summary.html); see the Supplemental Data for detailed procedures (http://www.neuron.org/cgi/content/full/42/2/237/DC1.

Muscle Electrophysiology

Electromyography was performed on anesthetized mice using stainless steel needles as described in detail in the Supplemental Data (http://www.neuron.org/cgi/content/full/42/2/237/DC1.

Morphological Analyses

For light microscopy of the NMJ, tibialis muscles were fixed in 1% PFA/PBS for 20 min, cryoprotected in sucrose, frozen, and sectioned en face at 40 μm in a cryostat. Sections were stained overnight with monoclonal antibodies to neurofilaments (SMI32; Sternberger) and SV2 (Developmental Studies Hybridoma Bank), washed, and then stained with secondary antibody (Alexa488 conjugated Goat anti-mouse IgG1; Molecular probes) and Rhodamine-labeled BTX (Molecular Probes). For ultrastructural studies, sternocleidomastoid muscles were fixed in 4% glutaraldehyde/4% PFA in PBS, washed, refixed in 1% OsO_4, dehydrated, and embedded in resin. Thin sections were stained with lead citrate and uranyl acetate, systematically scanned in the electron microscope, and all NMJs encountered in the micrographs were measured, with muscles from two to three animals analyzed per genotype and age. For immunocytochemistry at the Calyx of Held, brainstems were immersion fixed overnight in PBS containing 4% PFA, and vibratome sections (70–90 μm thick) were examined by immunofluorescence with a polyclonal anti-CSPα antibody (R807). For ultrastructural analyses of Calyx synapses, fresh brainstem vibratome sections (200 μm thick) were fixed with 2.5% glutaraldehyde/1% PFA in PBS and embedded in resin (Schoch et al., 2002) ($n = 4$ animals per genotype). Sections were analyzed with a Tecnai 12 Biotwin transmission electron microscope (FEI). Quantifications were performed with the Analysis Software (SIS).

Electrophysiological Recordings from the Calyx of Held

All recordings were performed at room temperature on transverse brainstem slices from littermate offspring of heterozygous matings. Recordings were obtained in standard extracellular bicarbonate-buffered Ringer's solution with 2 mM $CaCl_2$ and 1 mM $MgCl_2$ (Meyer et al., 2001); for presynaptic Ca^{2+} current recordings, 1 μM TTX, 10 mM TEA, 2 μM NBQX, and 50 μM D-APV were added, without or with ω-Agatoxin-IVa (Peptide Institute, Osaka, Japan) or ω-Conotoxin GVIA (Bachem, Heidelberg, Germany). Intracellular recording solutions contained (in mM) 130 Cs-gluconate, 10 Cs-HEPES, 20 TEA-Cl, 5 Na-phosphocreatine, 4 Mg-ATP, 0.3 Na_2GTP, with addition of 5 mM EGTA and 0.1 mM fura-2 for Ca^{2+} current recordings (Figure 4). After each recording, the presynaptic locus of recording was confirmed by taking fluorescence images of the fura-2-filled presynaptic calyces. Ca^{2+} currents are shown after a P/4 correction. Paired recordings were obtained with 0.5 and 5 mM EGTA, respectively, in pre- and postsynaptic intracellular solutions, and 1 μM TTX, 10 mM TEA, 50 μM D-APV, 100 μM cyclothiazide, and 1 mM kynurenic acid in extracellular solutions. The pre- and postsynaptic series resistances were compensated by up to 80%, and remaining series resistance errors (<30%) were compensated offline for EPSC traces (Meyer et al., 2001). Transmitter release rates were obtained by deconvolution of EPSCs (Neher and Sakaba, 2001), integrated, and fitted with double-exponential functions. Afferent fiber stimulations were made in the presence of 2 μM strychnine and 10 μM bicuculline with a concentric bipolar stimulation electrode (MCE 100; Rhodes Medical Instrument, Woodland Hills, CA) placed between the midline of the slice and the medial border of the MNTB. Cells that showed a pre- and postsynaptic spike in extracellular recordings after afferent fiber stimulation were selected for whole-cell recording (Borst et al., 1995; Meyer et al., 2001). Spontaneously occurring mEPSCs were recorded in 10 s intervals between stimulus trains of evoked EPSCs. mEPSCs were detected with a template matching routine (kindly provided by Dr. H. Taschenberger).

Miscellaneous

Most antibodies that were used were described previously (Rosahl et al., 1995; Schoch et al., 2002); antibodies to CSPα were raised to a GST-fusion protein of CSPα (R807) and are also previously described (Tobaben et al., 2001), or purchased from Stressgen Biotechnologies (Vancouver, Canada; VAP-SV003). All data are reported as mean ± SD, unless noted otherwise.

Acknowledgments

We thank R.E. Hammer, N. Korogod, J. Cunningham, I. Kornblum, E. Borowicz, J. Kiessling, C. de Cires, A. Roth, and P. Bronk for help, technical support, and advice. This study was supported by grants from the Deutsche Forschungsgemeinschaft (SFB-406, Schn 451/4-1 to R.S., and Schm 797/5-4 to F.S.), the Spanish Fondo de Investigaciones Sanitarias (01/1098) and the EMBO-Young Investigator Programme (to R.F.-C.), JA 2002/917 (to L.T.), a BEFI Fellowship (01/9310; to M.C.-M.), Heisenberg Fellowships (to R.S. and C.R.), and the N.I.H. (to J.R.S.).

Received: August 26, 2003
Revised: February 17, 2004
Accepted: March 5, 2004
Published: April 21, 2004

References

Borst, J.G., and Sakmann, B. (1996). Calcium influx and transmitter release in a fast CNS synapse. Nature *383*, 431–434.

Borst, J.G.G., Helmchen, F., and Sakmann, B. (1995). Pre- and postsynaptic whole-cell recordings in the medial nucleus of the trapezoid body of the rat. J. Physiol. *489*, 825–840.

Braun, J.E., Wilbanks, S.M., and Scheller, R.H. (1996). The cysteine string secretory vesicle protein activates Hsc70 ATPase. J. Biol. Chem. *271*, 25989–25993.

Bronk, P., Wenniger, J.J., Dawson-Scully, K., Guo, X., Hong, S., Atwood, H.L., and Zinsmaier, K.E. (2001). Drosophila Hsc70–4 is critical for neurotransmitter exocytosis in vivo. Neuron *30*, 475–488.

Brown, H., Larsson, O., Branstrom, R., Yang, S.N., Leibiger, B., Leibiger, I., Fried, G., Moede, T., Deeney, J.T., Brown, G.R., et al. (1998). Cysteine string protein (CSP) is an insulin secretory granule-associated protein regulating beta-cell exocytosis. EMBO J. *17*, 5048–5058.

Chamberlain, L.H., and Burgoyne, R.D. (1996). Identification of a novel cysteine string protein variant and expression of cysteine string proteins in non-neuronal cells. J. Biol. Chem. *271*, 7320–7323.

Chamberlain, L.H., and Burgoyne, R.D. (1997). Activation of the ATPase activity of heat-shock proteins Hsc70/Hsp70 by cysteine-string protein. Biochem. J. *322*, 853–858.

Chamberlain, L.H., and Burgoyne, R.D. (1998). Cysteine string protein functions directly in regulated exocytosis. Mol. Biol. Cell *9*, 2259–2267.

Chen, S., Zheng, X., Schulze, K.L., Morris, T., Bellen, H., and Stanley, E.F. (2002). Enhancement of presynaptic calcium current by cysteine string protein. J. Physiol. *538*, 383–389.

Dawson-Scully, K., Bronk, P., Atwood, H.L., and Zinsmaier, K.E. (2000). Cysteine-string protein increases the calcium sensitivity of neurotransmitter exocytosis in Drosophila. J. Neurosci. *20*, 6039–6047.

Evans, G.J., and Morgan, A. (2002). Phosphorylation-dependent interaction of the synaptic vesicle proteins cysteine string protein and synaptotagmin I. Biochem. J. *364*, 343–347.

Fernández-Chacón, R., and Südhof, T.C. (1999). Genetics of synaptic vesicle function: towards the complete functional anatomy of an organelle. Annu. Rev. Physiol. *61*, 753–776.

Forsythe, I.D., and Barnes-Davies, M. (1993). The binaural auditory pathway: excitatory amino acid receptors mediate dual timecourse excitatory postsynaptic currents in the rat medial nucleus of the trapezoid body. Proc. R. Soc. Lond. B. Biol. Sci. *251*, 151–157.

Graham, M.E., and Burgoyne, R.D. (2000). Comparison of cysteine string protein (Csp) and mutant alpha-SNAP overexpression reveals a role for csp in late steps of membrane fusion in dense-core granule exocytosis in adrenal chromaffin cells. J. Neurosci. *20*, 1281–1289.

Gundersen, C.B., and Umbach, J.A. (1992). Suppression cloning of the cDNA for a candidate subunit of a presynaptic calcium channel. Neuron *9*, 527–537.

Hartl, F.U., and Hayer-Hartl, M. (2002). Molecular chaperones in the

cytosol: from nascent chain to folded protein. Science *295*, 1852–1858.

Heckmann, M., Adelsberger, H., and Dudel, J. (1997). Evoked transmitter release at neuromuscular junctions in wildtype and cysteine string protein null mutant larvae of Drosophila. Neurosci. Lett. *228*, 167–170.

Isaacson, J.S. (1998). GABAB receptor-mediated modulation of presynaptic currents and excitatory transmission at a fast central synapse. J. Neurophysiol. *80*, 1571–1576.

Ishikawa, T., Sahara, Y., and Takahashi, T. (2002). A single packet of transmitter does not saturate postsynaptic glutamate receptors. Neuron *34*, 613–621.

Iwasaki, S., and Takahashi, T. (2001). Developmental regulation of transmitter release at the calyx of Held in rat auditory brainstem. J. Physiol. *534*, 861–871.

Iwasaki, S., Momiyama, A., Uchitel, O.D., and Takahashi, T. (2000). Developmental changes in calcium channel types mediating central synaptic transmission. J. Neurosci. *20*, 59–65.

Janz, R., Goda, Y., Geppert, M., Missler, M., and Südhof, T.C. (1999). SV2A and SV2B function as redundant Ca^{2+} regulators in neurotransmitter release. Neuron *24*, 1003–1016.

Jirmanova, I. (1975). Ultrastructure of motor end-plates during pharmacologically-induced degeneration and subsequent regeneration of skeletal muscle. J. Neurocytol. *4*, 141–155.

Joshi, I., and Wang, L.-Y. (2002). Developmental profiles of glutamate receptors and synaptic transmission at a single synapse in the mouse auditory brainstem. J. Physiol. *540*, 861–873.

Katz, B. (1969). The Release of Neural Transmitter Substances (Liverpool: Liverpool University Press).

Kelley, W.L. (1998). The J-domain family and the recruitment of chaperone power. Trends Biochem. Sci. *23*, 222–227.

Lenn, N.J., and Reese, T.S. (1966). The fine structure of nerve endings in the nucleus of the trapezoid body and the ventral cochlear nucleus. Am. J. Anat. *118*, 375–389.

Leveque, C., Pupier, S., Marqueze, B., Geslin, L., Kataoka, M., Takahashi, M., De Waard, M., and Seagar, M. (1998). Interaction of cysteine string proteins with the alpha1A subunit of the P/Q-type calcium channel. J. Biol. Chem. *273*, 13488–13492.

Magga, J.M., Jarvis, S.E., Arnot, M.I., Zamponi, G.W., and Braun, J.E. (2000). Cysteine string protein regulates G protein modulation of N-type calcium channels. Neuron *28*, 195–204.

Matos, M.F., Rizo, J., and Südhof, T.C. (2000). The relation of protein binding to function: what is the significance of munc18 and synaptotagmin binding to syntaxin *1*, and where are the corresponding binding sites? Eur. J. Cell Biol. *79*, 377–382.

Meyer, A.C., Neher, E., and Schneggenburger, R. (2001). Estimation of quantal size and number of functional active zones at the calyx of held synapse by nonstationary EPSC variance analysis. J. Neurosci. *21*, 7889–7900.

Morales, M., Ferrus, A., and Martinez-Padron, M. (1999). Presynaptic calcium-channel currents in normal and csp mutant Drosophila peptidergic terminals. Eur. J. Neurosci. *11*, 1818–1826.

Neher, E., and Sakaba, T. (2001). Combining deconvolution and noise analysis for the estimation of transmitter release rates at the calyx of held. J. Neurosci. *21*, 444–461.

Nie, Z., Ranjan, R., Wenniger, J.J., Hong, S.N., Bronk, P., and Zinsmaier, K.E. (1999). Overexpression of cysteine-string proteins in Drosophila reveals interactions with syntaxin. J. Neurosci. *19*, 10270–10279.

Patton, B.L., Chiu, A.Y., and Sanes, J.R. (1998). Synaptic laminin prevents glial entry into the synaptic cleft. Nature *393*, 698–701.

Patton, B.L., Cunningham, J.M., Thyboll, J., Kortesmaa, J., Westerblad, H., Edstrom, L., Tryggvason, K., and Sanes, J.R. (2001). Properly formed but improperly localized synaptic specializations in the absence of laminin α4. Nat. Neurosci. *4*, 597–604.

Ranjan, R., Bronk, P., and Zinsmaier, K.E. (1998). Cysteine string protein is required for calcium secretion coupling of evoked neurotransmission in Drosophila but not for vesicle recycling. J. Neurosci. *18*, 956–964.

Rogers, D.C., Fisher, E.M., Brown, S.D., Peters, J., Hunter, A.J., and Martin, J.E. (1997). Behavioral and functional analysis of mouse phenotype: SHIRPA, a proposed protocol for comprehensive phenotype assessment. Mamm. Genome *8*, 711–713.

Rosahl, T.W., Spillane, D., Missler, M., Herz, J., Selig, D.K., Wolff, J.R., Hammer, R.E., Malenka, R.C., and Südhof, T.C. (1995). Essential functions of synapsins I and II in synaptic vesicle regulation. Nature *375*, 488–493.

Sätzler, K., Sohl, L.F., Bollmann, J.H., Borst, J.G., Frotscher, M., Sakmann, B., and Lübke, J.H. (2002). Three-dimensional reconstruction of a calyx of Held and its postsynaptic principal neuron in the medial nucleus of the trapezoid body. J. Neurosci. *22*, 10567–10579.

Sakaba, T., and Neher, E. (2001). Calmodulin mediates rapid recruitment of fast-releasing synaptic vesicles at a calyx-type synapse. Neuron *32*, 1119–1131.

Sanes, J.R., and Lichtman, J.W. (1999). Development of the vertebrate neuromuscular junction. Annu. Rev. Neurosci. *22*, 389–442.

Schoch, S., Castillo, P.E., Jo, T., Mukherjee, K., Geppert, M., Wang, Y., Schmitz, F., Malenka, R.C., and Südhof, T.C. (2002). RIM1α forms a protein scaffold for regulating neurotransmitter release at the active zone. Nature *415*, 321–326.

Selkoe, D.J. (2002). Alzheimer's disease is a synaptic failure. Science *298*, 789–791.

Stanley, E.F. (1991). Single calcium channels on a cholinergic presynaptic nerve terminal. Neuron *7*, 585–591.

Südhof, T.C. (2004). The synaptic vesicle cycle. Ann. Rev. Neurosci. *27*, 509–547.

Takahashi, T., Forsythe, I.D., Tsujimoto, T., Barnes-Davies, M., and Onodera, K. (1996). Presynaptic calcium current modulation by a metabotropic glutamate receptor. Science *274*, 594–597.

Takahashi, T., Kajikawa, Y., and Tsujimoto, T. (1998). G-Protein-coupled modulation of presynaptic calcium currents and transmitter release by a GABAB receptor. J. Neurosci. *18*, 3138–3146.

Taschenberger, H., and von Gersdorff, H. (2000). Fine-tuning an auditory synapse for speed and fidelity: Developmental changes in presynaptic waveform, EPSC kinetics, and synaptic plasticity. J. Neurosci. *20*, 9162–9173.

Taschenberger, H., Leao, R.M., Rowland, K.C., Spirou, G.A., and von Gersdorff, H. (2002). Optimizing synaptic architecture and efficiency for high-frequency transmission. Neuron *36*, 1127–1143.

Tobaben, S., Thakur, P., Fernandez-Chacon, R., Sudhof, T.C., Rettig, J., and Stahl, B. (2001). A trimeric protein complex functions as a synaptic chaperone machine. Neuron *31*, 987–999.

Umbach, J.A., Zinsmaier, K.E., Eberle, K.K., Buchner, E., Benzer, S., and Gundersen, C.B. (1994). Presynaptic dysfunction in Drosophila csp mutants. Neuron *13*, 899–907.

Umbach, J.A., Saitoe, M., Kidokoro, Y., and Gundersen, C.B. (1998). Attenuated influx of calcium ions at nerve endings of csp and shibire mutant Drosophila. J. Neurosci. *18*, 3233–3240.

von Gersdorff, H., Schneggenburger, R., Weis, S., and Neher, E. (1997). Presynaptic depression at a calyx synapse: The small contribution of metabotropic glutamate receptors. J. Neurosci. *17*, 8137–8146.

Wang, L.-Y., and Kaczmarek, L.K. (1998). High-frequency firing helps replenish the readily releasable pool of synaptic vesicles. Nature *394*, 384–388.

Wu, L.G., Westenbroek, R.E., Borst, J.G., Catterall, W.A., and Sakmann, B. (1999). Calcium channel types with distinct presynaptic localization couple differentially to transmitter release in single calyx-type synapses. J. Neurosci. *19*, 726–736.

Yawo, H., and Chuhma, N. (1994). ω-conotoxin-sensitive and -resistant transmitter release from the chick ciliary presynaptic terminal. J. Physiol. *477*, 437–448.

Zhang, H., Kelley, W.L., Chamberlain, L.H., Burgoyne, R.D., Wollheim, C.B., and Lang, J. (1998). Cysteine-string proteins regulate exocytosis of insulin independent from transmembrane ion fluxes. FEBS Lett. *437*, 267–272.

Zinsmaier, K.E., Hofbauer, A., Heimbeck, G., Pflugfelder, G.O., Buchner, S., and Buchner, E. (1990). A cysteine-string protein is expressed in retina and brain of Drosophila. J. Neurogenet. *7*, 15–29.

Zinsmaier, K.E., Eberle, K.K., Buchner, E., Walter, N., and Benzer, S. (1994). Paralysis and early death in cysteine string protein mutants of Drosophila. Science *263*, 977–980.